

**High-spin states in  $^{90}\text{Ru}$  and the projected shell model description**

D. Bucurescu,<sup>1</sup> N. Mărginean,<sup>2,1</sup> C. Rossi Alvarez,<sup>3</sup> Y. Sun,<sup>4,5</sup> C. A. Ur,<sup>3,1</sup> L. C. Mihăilescu,<sup>1</sup> G. Suliman,<sup>1</sup> D. Bazzacco,<sup>3</sup> S. Lunardi,<sup>3</sup> G. de Angelis,<sup>2</sup> M. Axiotis,<sup>2</sup> E. Farnea,<sup>3</sup> A. Gadea,<sup>2</sup> M. Ionescu-Bujor,<sup>1</sup> A. Iordăchescu,<sup>1</sup> W. Krolas,<sup>6</sup> Th. Kröll,<sup>7</sup> S. M. Lenzi,<sup>3</sup> T. Martinez,<sup>2</sup> R. Menegazzo,<sup>3</sup> D. R. Napoli,<sup>2</sup> P. Pavan,<sup>3</sup> Zs. Podolyak,<sup>8</sup> C. Rusu,<sup>2</sup> M. De Poli,<sup>2</sup> B. Quintana,<sup>9</sup> and P. Spolaore<sup>2</sup>

<sup>1</sup>*H. Hulubei National Institute for Physics and Nuclear Engineering, Bucharest, Romania*

<sup>2</sup>*INFN, Laboratori Nazionali di Legnaro, Italy*

<sup>3</sup>*Dipartimento di Fisica dell'Università and INFN, Sezione di Padova, Italy*

<sup>4</sup>*Department of Physics and Joint Institute for Nuclear Astrophysics, University of Notre Dame, Notre Dame, Indiana 46556, USA*

<sup>5</sup>*Department of Physics, Xuzhou Normal University, Xuzhou, Jiangsu 221009, People's Republic of China*

<sup>6</sup>*Institute of Nuclear Physics, Krakow, Poland*

<sup>7</sup>*Physik Department E12, Technische Universität München, Garching, Germany*

<sup>8</sup>*Department of Physics, University of Surrey, Guildford GU2 7XH, UK*

<sup>9</sup>*Grupo de Física Nuclear, Universidad de Salamanca, Spain*

(Received 9 February 2004; published 21 June 2004)

The neutron deficient  $A \sim 90$  nuclei constitute a good testing ground for shell model approaches based on spherical or deformed basis. New experimental data are presented for the  $^{90}\text{Ru}$  nucleus, as obtained with the reaction  $^{40}\text{Ca} + ^{58}\text{Ni}$  at 135 MeV. The yrast band has been extended to higher spin states and a new band, tentatively assigned as a negative parity band, has been identified. The observed structures are compared with predictions of the projected shell model, which uses a deformed basis. Possibility of the occurrence of low-lying high- $K$  states in this nucleus is discussed.

DOI: 10.1103/PhysRevC.69.064319

PACS number(s): 21.10.Re, 23.20.Lv, 25.70.Jj, 27.60.+j

**I. INTRODUCTION**

The nuclei near the  $N=50$  shell closure constitute a traditional ground for testing different shell model calculations, and for extracting information on the residual interactions [1–4]. For example, the early calculations of Gross and Frenkel [2], within the restricted model space ( $2p_{1/2}$  and  $1g_{9/2}$ ) and using an empirical interaction, were successful for the  $N=48-50$  nuclei. The study was later extended to the nuclei away from the shell closure by using the same model space [5,6]. However, when a similar study was applied for the  $N=46$  nuclei [7,8], it showed a generally weaker agreement with the measurements than that found for the  $N>47$  nuclei. One of the reasons for the discrepancy might be the restriction in the configuration space when performing the shell model calculations. Indeed, the very recent shell model calculations of Hasegawa *et al.* [9], in which a larger space ( $2p_{3/2}, 1f_{5/2}, 2p_{1/2}, 1g_{9/2}$ ) is used, have been able to reproduce the known high spin data in  $^{90}\text{Ru}$ .

A study of the  $N=46$  nuclei is especially interesting since it appears that near this neutron number the structure changes rapidly from the spherical to the deformed type [10]. For the shell model based on a spherical basis, the configuration space needed for these nuclei (as employed in [9]) is huge, and it approaches the limit of what can be presently handled for this mass region. On the other hand, the shell models based on a deformed basis, such as the projected shell model [11], will gradually lose the advantages when moving from the well-deformed (Zr) to the spherical (Sn) region. Thus, the nucleus  $^{90}\text{Ru}$  is among a limited number of cases where both types of shell model, spherical- and deformed-based, can be applied, and thus can be tested comparatively against data.

To test various theoretical predictions, more detailed experimental information of these nuclei, such as that of high spin states and non-yrast bands, is very much desired. The nucleus  $^{90}\text{Ru}$  was studied before with a heavy-ion fusion-evaporation reaction [7], its yrast line being observed up to 6.4 MeV in excitation and  $16^+$  in spin. In this work we extend the experimental level scheme of the yrast band, and present a new band with negative parity. These data are compared in detail with calculations performed with the projected shell model.

The experimental results for  $^{90}\text{Ru}$  will be presented in Sec. II, with an illustration of the systematics of band structures with both positive and negative parity in several  $N=46$  isotones. In Sec. III, the data will be compared with the predictions of the projected shell model. From the same calculation, there appear some low-lying high- $K$  bands in  $^{90}\text{Ru}$ , which will also be discussed. Finally, the paper will be summarized in Sec. IV.

**II. THE EXPERIMENT**

The  $^{90}\text{Ru}$  nucleus has been populated in the  $^{40}\text{Ca} + ^{58}\text{Ni}$  reaction, performed with a  $^{40}\text{Ca}$  beam of 135 MeV delivered by the Legnaro XTU Tandem accelerator. The beam intensity was around 8 particle nA and the target was a 6 mg/cm<sup>2</sup>  $^{58}\text{Ni}$  foil. The  $\gamma$ -rays were detected with the GASP array [12] in its standard configuration with 40 Compton-suppressed HPGe detectors and an 80 BGO element inner ball, and the trigger condition was that at least two Ge detectors and one BGO fired in coincidence. More details of this experiment are given in Refs. [13,14]. Important for the present study of  $^{90}\text{Ru}$  (populated through the  $2\alpha$  channel) is the use of the

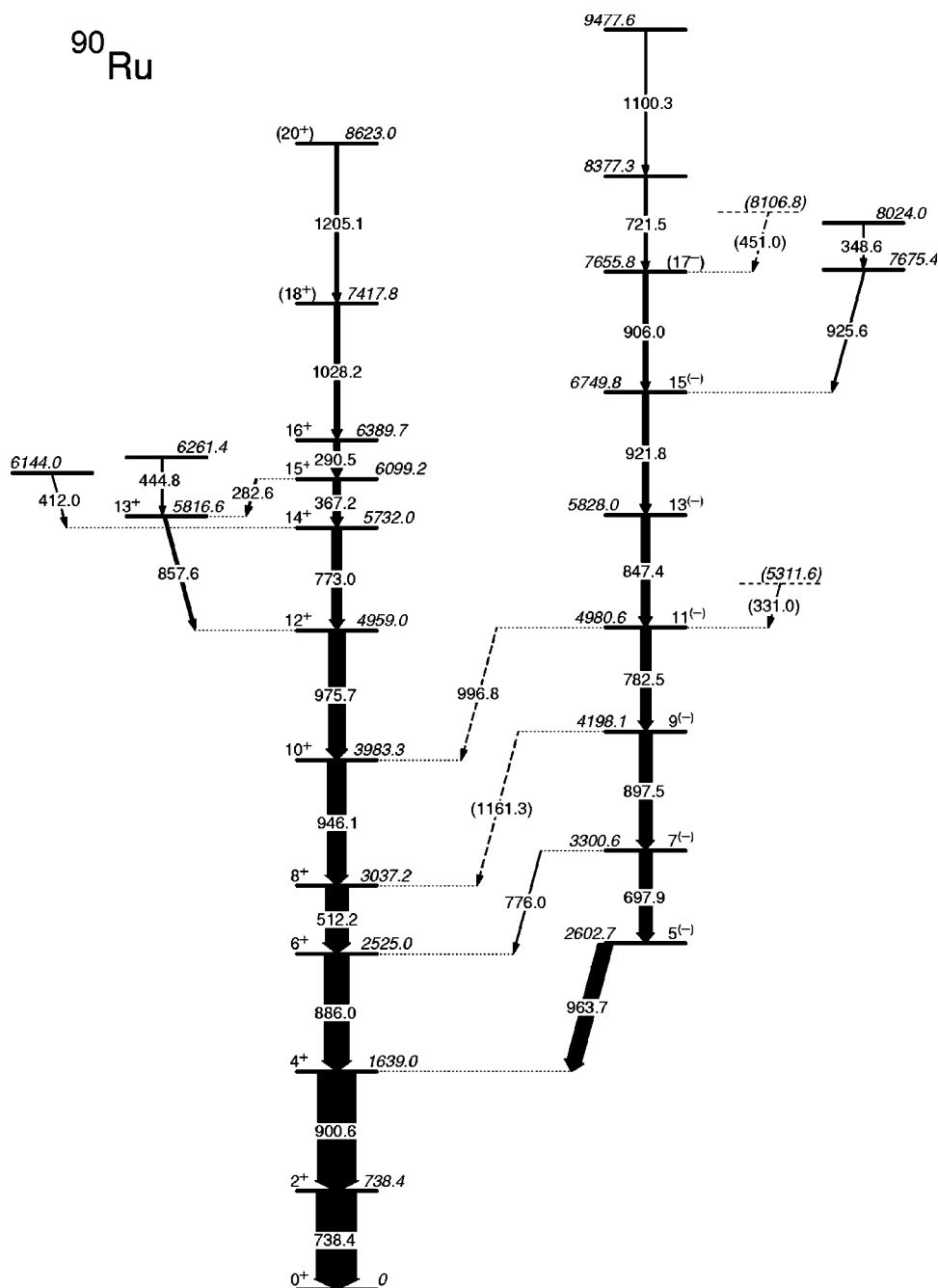


FIG. 1. Level scheme of  $^{90}\text{Ru}$  as determined from the present experiment. For details see text and Table I.

ISIS Silicon ball [15], an array of 40  $\Delta E$ - $E$  telescopes arranged in a geometry similar to that of GASP. The  $\Delta E$  detectors were protected by absorbing foils such as to remove the scattered Ca beam, the final efficiency obtained for the detection of one  $\alpha$ -particle being of 38%. Gating  $\gamma$ - $\gamma$  coincidences with two  $\alpha$ -particles selected practically only the transitions from  $^{90}\text{Ru}$ . The level scheme of this nucleus has therefore been very conveniently constructed, by starting from the known yrast transitions [7] and working on a symmetric  $\gamma$ - $\gamma$ - $\gamma$  cube or a  $\gamma$ - $\gamma$  matrix sorted with this condition.

Figure 1 shows the level scheme obtained from this experiment. Figure 2 shows a few spectra obtained from  $\gamma$ -ray windows on the symmetric  $\gamma$ - $\gamma$  matrix gated by two  $\alpha$ -particles, which illustrate the two band structures from

Fig. 1. Information on the multiplicities of the  $\gamma$ -ray transitions could be deduced from  $\gamma$ -ray angular distributions and directional correlation orientation (DCO) ratios. The  $\gamma$ -ray angular distributions were extracted from spectra of the seven rings of GASP detectors, gated by two  $\alpha$ -particles. The relative intensities of the gamma-ray transitions, as well as the Legendre polynomial coefficients of their angular distributions are given in Table I. The DCO ratios, also given in Table I, have been determined from an asymmetric  $\gamma$ - $\gamma$  matrix coincident with one  $\alpha$  particle, in which the energy of the  $\gamma$ -rays detected in the detector rings at  $35^\circ$  or  $145^\circ$  was recorded on one axis, while that of the  $\gamma$ -rays detected at  $72^\circ$ ,  $90^\circ$ , or  $108^\circ$  was recorded on the other axis. By including the two rings closest to  $90^\circ$  the efficiency of the procedure was increased. The DCO ratios were determined as

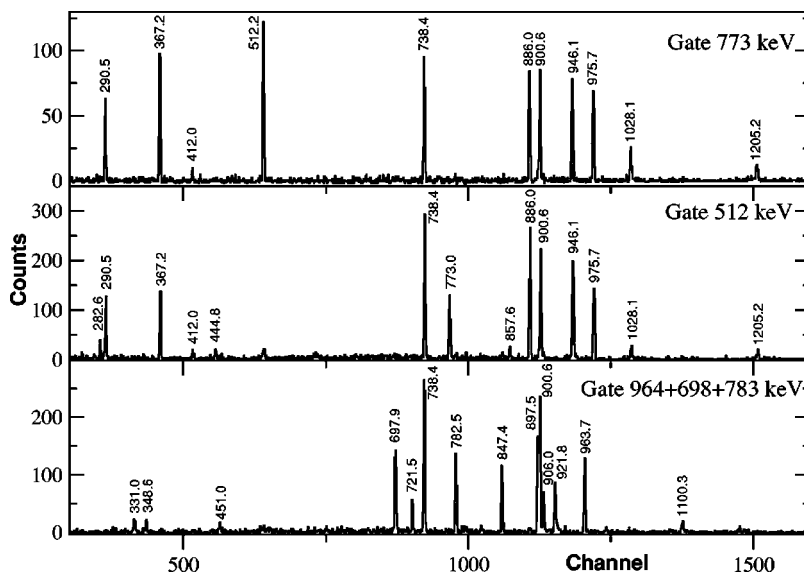


FIG. 2. Examples of  $\gamma$ -ray coincidence relationships. The spectra are obtained by gating on the specified transitions, on a  $\gamma$ - $\gamma$  symmetric matrix coincident with two  $\alpha$ -particles.

$$R_{\text{DCO}} = \frac{I(\gamma_1 \text{ at } 72^\circ \text{ or } 90^\circ \text{ or } 108^\circ; \gamma_2 \text{ at } 35^\circ \text{ or } 145^\circ)}{I(\gamma_1 \text{ at } 35^\circ \text{ or } 145^\circ; \gamma_2 \text{ at } 72^\circ \text{ or } 90^\circ \text{ or } 108^\circ)}$$

If the gating transition  $\gamma_1$  is of stretched quadrupole type, the DCO ratio of the  $\gamma_2$  transition is expected to be about 0.5 for a stretched dipole transition, and about 1.0 for a stretched quadrupole transition; this was checked on transitions of known multiplicities.

The positive parity yrast line up to the  $16^+$  state contains the same transitions as observed in Ref. [7]. Nevertheless, on the basis of our intensities (Table I) we have interchanged the positions of the 886 and 946 keV transitions. Some yrare positive parity transitions and two transitions above the  $16^+$  state have been added; also, we have established the spin-parity  $14^+$  for the  $E_x=5732$  keV state, previously assigned as  $(13^+, 14^+)$ , and observed the new state at 5817 keV, assigned as  $13^+$ . Figure 3 shows systematic trends of the levels observed in the  $N=46$  isotones  $^{86}\text{Zr}$  [16],  $^{88}\text{Mo}$  [17], and  $^{90}\text{Ru}$  (this work). The new placement of the 886 and 946 keV transitions from the ground state band of  $^{90}\text{Ru}$  leads to a smoother systematic of this band. As seen in Fig. 1, a new band which feeds the  $4^+$  yrast state has been established. Its spin values (Fig. 1) were assigned on the basis of the angular distribution and DCO ratio data (Table I). This band continues smoothly the systematic of a negative parity band well established in the lighter isotones, and therefore, we have tentatively assigned it as a negative parity band. The two transitions in the upper part of this structure (722 and 1100 keV) have both the angular distribution coefficients and the DCO ratios with larger errors, which did not allow a multipolarity assignment.

### III. THE PROJECTED SHELL MODEL DESCRIPTION

A description of the positive-parity yrast levels in  $^{90}\text{Ru}$  with a spherical shell model approach has been presented in detail in three previous papers [7–9]. The calculations in Refs. [7,8] considered the  $2p_{1/2}$  and  $1g_{9/2}$  subshells outside a semimagic  $^{88}\text{Sr}$  core as the model space, and used the single-

particle energies and two-body matrix elements of Gross and Frenkel [2]. The order of the  $13^+$  and  $14^+$  states (see Fig. 1) was well predicted by these calculations, and the decay of the  $15^+$  state towards both these states was reasonably well described [7]. A negative parity structure was also predicted [8], starting around the excitation energy of 3.2 MeV. On the other hand, the calculated positive-parity yrast band, shown in both cited papers [7,8], was more compressed than the observed one. Improved agreement for the  $^{90}\text{Ru}$  yrast band was obtained by the recent shell model calculation [9], in which an enlarged model space ( $2p_{3/2}, 1f_{5/2}, 2p_{1/2}, 1g_{9/2}$ ) and an extended pairing plus quadrupole interaction were employed. In the following, we discuss the observed structure of  $^{90}\text{Ru}$  within the framework of the projected shell model.

#### A. The calculation conditions

In contrast to the spherical shell models [7–9], the projected shell model (PSM) builds its model basis by using

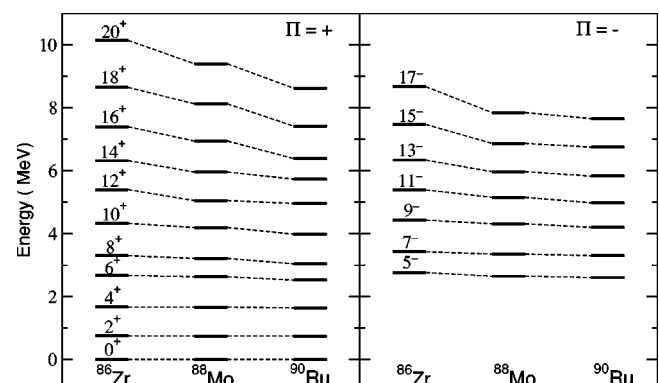


FIG. 3. Systematics of band structures in the  $N=46$  isotones. The data for  $^{86}\text{Zr}$  are from Ref. [16], those for  $^{88}\text{Mo}$  from Ref. [17]. The band observed in the present work above the state with spin 5 at  $E_x=2603$  keV is very similar to the negative parity bands known in the lighter isotones, and is therefore tentatively proposed as the analogue negative parity band.

TABLE I. Energies and relative intensities of the  $\gamma$ -ray transitions assigned to  $^{90}\text{Ru}$  (level scheme of Fig. 1). For the stronger transitions the angular distribution coefficients  $a_2/a_0$  and  $a_4/a_0$ , as well as the DCO ratios (see text for details) are also given. The errors in the transition energies are below 0.3 keV.

$E_\gamma$ (keV)	$I_\gamma$	$a_2/a_0$	$a_4/a_0$	$R_{\text{DCO}}$	$J_i^\pi$	$J_f^\pi$	$E_i$	$E_f$
282.6	3.8(6)	0.41(26)	0.10(31)		15 <sup>+</sup>	13 <sup>+</sup>	6099.2	5816.6
290.5	15.0(14)	-0.37(14)	-0.03(18)	0.46(10) <sup>d</sup>	16 <sup>+</sup>	15 <sup>+</sup>	6389.7	6099.2
331.0						11 <sup>(-)</sup>	5311.6	4980.6
348.6	2.6(8)						8024.0	7675.4
367.2	17.9(19)	-0.31(14)	0.09(31)	0.62(9) <sup>e</sup>	15 <sup>+</sup>	14 <sup>+</sup>	6099.2	5732.0
412.0	2.0(5)				14 <sup>+</sup>	6144.0	5732.0	
444.8	2.7(8)				13 <sup>+</sup>	6261.4	5816.6	
451.0					(17 <sup>-</sup> )	8106.8	7655.8	
512.2	57.4(40)	0.35(12)	0.16(18)	0.93(5) <sup>d</sup>	8 <sup>+</sup>	6 <sup>+</sup>	3037.2	2525.0
697.9	32.2(38)	0.23(23)	-0.19(33)	1.04(7) <sup>a</sup>	7 <sup>(-)</sup>	5 <sup>(-)</sup>	3300.6	2602.7
721.5	6.9(12)	0.04(22)	-0.26(33)	0.95(18) <sup>a</sup>		(17 <sup>-</sup> )	8377.1	7655.6
738.4	100	0.27(14)	-0.01(18)	1.04(6) <sup>b</sup>	2 <sup>+</sup>	0 <sup>+</sup>	738.4	0.0
773.0	24.9(26)	0.30(10)	0.04(16)	1.16(20) <sup>e</sup>	14 <sup>+</sup>	12 <sup>+</sup>	5732.0	4959.0
776.0	2.2(14)				7 <sup>(-)</sup>	6 <sup>+</sup>	3300.6	2525.0
782.5	26.5(41)	0.27(9)	-0.09(14)	1.06(11) <sup>a</sup>	11 <sup>(-)</sup>	9 <sup>(-)</sup>	4980.6	4198.1
847.4	20.6(35)	0.44(15)	0.02(24)	0.86(12) <sup>a</sup>	13 <sup>(-)</sup>	11 <sup>(-)</sup>	5828.0	4980.6
857.6	7.1(12)	-0.11(23)	0.77(54)	0.46(12) <sup>f</sup>	13 <sup>+</sup>	12 <sup>+</sup>	5816.6	4959.0
886.0	61.3(48)	0.26(10)	-0.03(16)	1.00(11) <sup>a</sup>	6 <sup>+</sup>	4 <sup>+</sup>	2525.0	1639.0
897.5	32.1(51)	0.14(8)	-0.21(12)	1.07(17) <sup>a</sup>	9 <sup>(-)</sup>	7 <sup>(-)</sup>	4198.1	3300.6
900.6	96.9(37)	0.20(5)	-0.10(8)	1.00(9) <sup>c</sup>	4 <sup>+</sup>	2 <sup>+</sup>	1639.0	738.4
906.0	10.8(16)	0.54(21)	0.27(20)	0.98(4) <sup>a</sup>	(17 <sup>-</sup> )	15 <sup>(-)</sup>	7655.8	6749.8
921.8	14.9(24)	0.28(24)	0.03(33)	0.92(26) <sup>a</sup>	15 <sup>(-)</sup>	13 <sup>(-)</sup>	6749.8	5828.0
925.6	3.3(9)					15 <sup>-</sup>	7675.4	6749.8
946.1	45.0(36)	0.19(16)	-0.08(21)	0.97(8) <sup>d</sup>	10 <sup>+</sup>	8 <sup>+</sup>	3983.3	3037.2
963.7	36.7(40)	-0.15(14)	0.62(30)	0.61(5) <sup>a</sup>	5 <sup>(-)</sup>	4 <sup>+</sup>	2602.7	1639.0
975.7	40.2(43)	0.28(9)	-0.10(18)	0.92(8) <sup>d</sup>	12 <sup>+</sup>	10 <sup>+</sup>	4959.0	3983.3
996.8	1.4(8)				11 <sup>(-)</sup>	10 <sup>+</sup>	4980.6	3983.3
1028.1	12.2(18)	0.23(28)	-0.05(43)	0.87(26) <sup>d</sup>	(18 <sup>+</sup> )	16 <sup>+</sup>	7417.8	6389.7
1100.3	3.9(10)	-0.19(26)	0.29(41)	0.89(30) <sup>a</sup>			9477.6	8377.3
1205.2	8.3(17)	0.15(18)	0.28(36)	1.09(22) <sup>d</sup>	(20 <sup>+</sup> )	(18 <sup>+</sup> )	8623.0	7417.8

<sup>a</sup>From gate on the transitions 738 and 901 keV.

<sup>b</sup>From gate on the transitions 901 and 886 keV.

<sup>c</sup>From gate on the transitions 738 and 886 keV.

<sup>d</sup>From gate on the transitions 738, 901, and 886 keV.

<sup>e</sup>From gate on the transition 976 keV.

<sup>f</sup>From gate on the transitions 976 and 946 keV.

deformed (Nilsson-type) quasiparticle states [11]. One advantage of this approach is that the dominant nuclear correlations can be incorporated efficiently in the wave functions. Therefore, the PSM can treat the well-deformed nuclei without running into problems related to dimension explosion. The deformed Nilsson states violate angular momentum. However, there are well established projection techniques which allow a recovery of this quantum number. Thus, a PSM wave function is a linear combination of the angular momentum projected states given by

$$|\psi_M^J\rangle = \sum_{\kappa} f_{\kappa} \hat{P}_{MK_{\kappa}}^J |\varphi_{\kappa}\rangle. \quad (1)$$

The intrinsic states  $|\varphi_{\kappa}\rangle$  are multi-quasiparticle (qp) states, which include 0-, 2-, and 4-qp configurations. The index  $\kappa$  labels the basis states. These multi-qp states carry the good  $K$  quantum number originated from the deformed Nilsson single-particle states.

The present calculations have been performed by taking into account three full major shells ( $N=2, 3, 4$ ) for both neu-

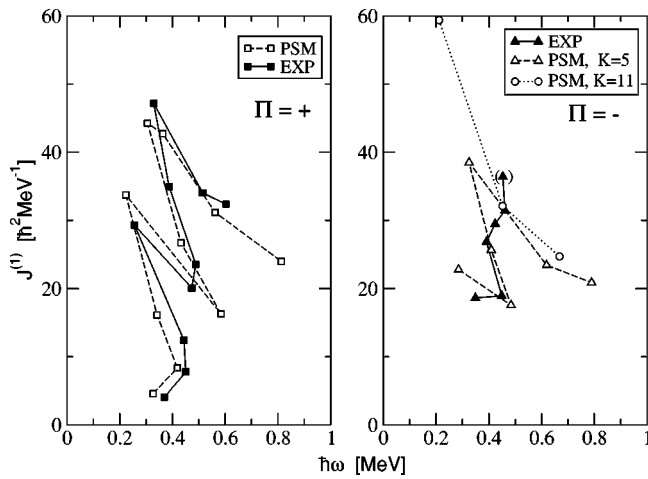


FIG. 4. Comparison of experimental kinematic moments of inertia of  $^{90}\text{Ru}$  band structures with the results of the projected shell model calculations.

trons and protons. This model space is far beyond what a spherical shell model can presently handle. The PSM employs the pairing plus quadrupole Hamiltonian, with the inclusion of a quadrupole-pairing term [11]. For the interaction strengths we have used the same standard values as those used in all the previous PSM studies [18–23] for this mass region, without any modification. Thus, we have a consistent theoretical framework for even-even, odd-A, and odd-odd nuclei. Our calculations are performed for  $^{90}\text{Ru}$  with the basis deformation  $\epsilon_2=0.16$ . It is interesting to mention that the fact that the PSM prefers the choice of such a deformed basis was discussed in the spherical shell model point of view [9].

**B. Comparison with the data**

The results of the PSM calculations are compared with the experimental data in Figs. 4 and 5. Figure 4 shows the typical cranking model representation, i.e., the moment of inertia versus the rotational frequency. For the positive parity yrast band, the two backbendings in the moment of inertia

are very well reproduced. There is an important change of structure above the  $14^+$  state, as indicated by the absence of the  $16^+ \rightarrow 14^+$  E2 transition, which is replaced by a cascade of two M1 transitions (Fig. 1).

The detailed analysis of the PSM results shows that the first backbending in the moment of inertia is attributed to the band-crossing of the neutron 2-qp band ( $K=1$ , from coupling two  $g_{9/2}$  neutrons having  $K=5/2$  and  $7/2$ ) with the 0-qp ground band. Thus, the crossing, occurring between  $I=4$  and 6, corresponds to the alignment of two  $g_{9/2}$  neutrons. Between  $I=10$  and 12, the results indicate another band-crossing of this neutron 2-qp band with a 4-qp band consisting of two  $g_{9/2}$  neutrons and two  $g_{9/2}$  protons. This corresponds to the alignment of a pair of  $g_{9/2}$  neutrons followed by that of the  $g_{9/2}$  protons, and explains the observed second backbending in the moment of inertia. The observed  $13^+$  and  $15^+$  states are also reasonably well predicted in energy. As seen in Fig. 5, the calculations predict another band-like structure based on a  $K=12$  state which, in the region of spins 12 to 15 is rather close in energy with the states from the yrast band. However, there is no important mixing between the states of this band and those of the yrast band.

The lower part of the band tentatively assigned as a negative parity one, is also well described by the PSM calculations, which predict a  $K=5$  band starting around the correct excitation energy (Fig. 5), whose backbending compares well with the experimental one (Fig. 4). The detailed analysis shows that before the backbending this band has a proton 2-qp structure, while after the backbending, its structure changes to a 4-qp one. The proton 2-qp state is mainly a  $K=5$  one (coupling of one  $g_{9/2}$  proton having  $K=5/2$  and one  $f_{5/2}$  proton having  $K=5/2$ ). It is however strongly mixed with another proton 2-qp state with  $K=6$  (coupling of one  $g_{9/2}$  proton having  $K=7/2$  and one  $f_{5/2}$  proton having  $K=5/2$ ). Galindo *et al.* [8] predicted a negative parity band in  $^{90}\text{Ru}$  having the bandhead at  $I=4$  and about 3.2 MeV. This must be a different band compared to our results since the  $f_{5/2}$  subshell was not considered in their model space. Concerning the 4-qp state configuration after the backbending, the calculations indicate a structure having a neutron  $g_{9/2}$  pair added to the proton 2-qp state. Thus, the observed backbend-

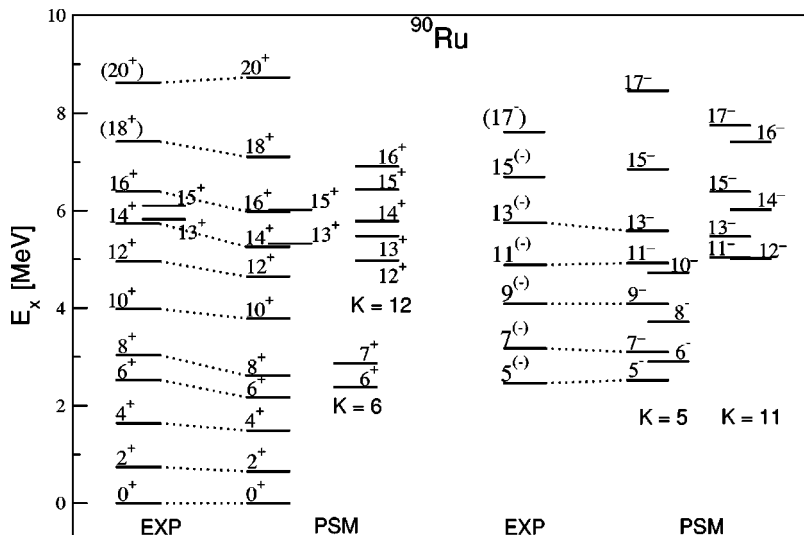


FIG. 5. Comparison of the experimental level scheme of  $^{90}\text{Ru}$  with the prediction of the projected shell model calculations (see text for comments on the predicted states which have no experimental counterparts).

ing in this negative parity sequence can be interpreted as an alignment of two  $g_{9/2}$  neutrons, which is the same mechanism that causes the first backbending in the positive parity yrast band.

At  $I=11$  in the negative parity sequence, the calculations predict the occurrence of a  $K=11$  band (Fig. 5). The bandhead of this high- $K$  band intrudes into the  $K=5$  band sequence and the states appear even lower in energy for  $I=13$  and beyond.

### C. A note on high- $K$ states

In the present PSM calculations, a  $K=6$  2-qp state is predicted particularly low in excitation energy. The state, having  $I^\pi=6^+$ , is predicted to lie at 2.38 MeV in excitation (Fig. 5). The structure of this state is the neutron 2-qp state coupled to two  $g_{9/2}$  neutrons having  $K=5/2$  and  $7/2$ . It is worth pointing out that these two  $g_{9/2}$  neutrons, when coupled to  $K=1$ , are responsible for the observed backbendings (Fig. 4), as discussed in the previous section. Prediction for this  $K=6$  isomer in some other  $N\sim Z$  nuclei in the  $A\sim 80-90$  mass region was given in [20]. Above the  $7^+$  state, the states belonging to this  $K=6$  structure are quite far from the yrast region.

The PSM calculations indicate that in  $^{90}\text{Ru}$  certain 4-qp high- $K$  states can also appear very close to the yrast line. Our calculations show that the predicted  $K=11$ ,  $I^\pi=11^-$  state (shown in the previous section) has an excitation energy of 5.13 MeV. It has a main structure which involves the two protons that make the negative parity  $K=5$  band and a  $K=6$  pair of  $g_{9/2}$  neutrons. Another 4-qp state appearing from the calculation has positive parity, and is predicted to lie at an excitation energy of 4.98 MeV, about 300 keV above the yrast line (Fig. 5). This  $K=12$ ,  $I^\pi=12^+$  state has a structure of

a pair of  $K=6$   $g_{9/2}$  neutrons plus a pair of  $K=6$   $g_{9/2}$  protons.

## IV. CONCLUSIONS

In this paper, we have reported new experimental data for  $^{90}\text{Ru}$ , as obtained with the reaction  $^{40}\text{Ca}+^{58}\text{Ni}$  at 135 MeV. The yrast band was extended to higher spin states, well beyond the second backbending. Another band has been identified for the first time and was tentatively assigned as having negative parity. The observed structures were compared with predictions of the projected shell model. Possible occurrence of high- $K$  isomers in this nucleus has been discussed.

The large amount of new experimental data in this mass region has been awaiting extended theoretical work. Within the spherical shell model framework, most of the early calculations were restricted in a very small space ( $1g_{9/2}, 2p_{1/2}$ ). However, effects of the nearby orbitals such as  $p_{3/2}, f_{5/2}, d_{5/2}$ , and  $g_{7/2}$  should be included to achieve a more comprehensive picture. At present, this is only possible through the use of a deformed basis supplemented by angular momentum projection. It is shown in this work that the projected shell model can give a reasonable description for the  $^{90}\text{Ru}$  data through a manageable amount of numerical effort. The prediction of high- $K$  isomeric states in  $^{90}\text{Ru}$  should, however, be tested by future experiments, and possibly be compared with spherical shell model calculations.

## ACKNOWLEDGMENTS

We acknowledge the support received within the European Contract No. HPRI-CT-1999-00083 - V Framework Programme. Y.S. acknowledges the support by the NSF under Contract No. PHY-0140324. We also acknowledge partial support through a research grant of the Romanian National University Research Council (CNCSIS).

- 
- [1] D. H. Gloeckner and F. J. D. Serduke, Nucl. Phys. **A220**, 477 (1974).
  - [2] R. Gross and A. Frenkel, Nucl. Phys. **A267**, 85 (1976).
  - [3] J. Blomquist and L. Rydstrom, Phys. Scr. **31**, 31 (1985).
  - [4] X. Ji and B. H. Wildenthal, Phys. Rev. C **37**, 1256 (1988).
  - [5] D. Rudolph, K. P. Lieb, and H. Grawe, Nucl. Phys. **A597**, 298 (1996).
  - [6] H. Herndl and B. A. Brown, Nucl. Phys. **A627**, 35 (1997).
  - [7] J. Heese *et al.*, Phys. Rev. C **49**, 1896 (1994).
  - [8] E. Galindo, A. Jungclauss, and K. P. Lieb, Eur. Phys. J. A **9**, 439 (2000).
  - [9] M. Hasegawa, K. Kaneko, T. Mizusaki, and S. Tazaki, Phys. Rev. C **69**, 034324 (2004).
  - [10] P. Moeller, J. R. Nix, W. D. Myers, and W. J. Swiatecki, At. Data Nucl. Data Tables **59**, 185 (1995).
  - [11] K. Hara and Y. Sun, Int. J. Mod. Phys. E **4**, 637 (1995).
  - [12] D. Bazzacco, Proceedings of the International Conference on Nuclear Structure at High Angular Momentum, Ottawa, 1992, Report No. AECL 10613, Vol. II, p. 376.
  - [13] N. Mărginean *et al.*, Phys. Rev. C **67**, 061301(R) (2003).
  - [14] C. Rusu *et al.*, Phys. Rev. C **69**, 024307 (2004).
  - [15] E. Farnea *et al.*, Nucl. Instrum. Methods Phys. Res. A **400**, 87 (1997).
  - [16] E. K. Warburton *et al.*, Phys. Rev. C **31**, 1211 (1985); J. Döring *et al.*, *ibid.* **61**, 034310 (2000).
  - [17] M. Weiszflog *et al.*, Z. Phys. A **342**, 257 (1992).
  - [18] R. Palit, J. A. Sheikh, Y. Sun, and H. C. Jain, Nucl. Phys. **A686**, 141 (2001).
  - [19] R. Palit, J. A. Sheikh, Y. Sun, and H. C. Jain, Phys. Rev. C **67**, 014321 (2003).
  - [20] Y. Sun, Eur. Phys. J. A **20**, 133 (2004).
  - [21] N. Mărginean *et al.*, Phys. Rev. C **65**, 051303(R) (2002).
  - [22] N. Mărginean *et al.*, Phys. Rev. C **65**, 034315 (2002).
  - [23] N. Mărginean *et al.*, Phys. Rev. C **69**, 054301 (2004).